Supplementary Materials for Parametric Excitation of a Bose-Einstein Condensate: From Faraday Waves to Granulation

J. H. V. Nguyen, M. C. Tsatsos, D. Luo, A. U. J. Lode, G. D. Telles , V. S. Bagnato, R. G. Hulet

EXPERIMENTAL DETAILS

A pair of coils in Helmholtz configuration is used to produce a homogeneous magnetic field, B, which allows us to vary the interatomic interactions. For a given value of B the corresponding scattering length is determined from:

$$a = a_{\mathrm{bg}}\left(1 + \frac{\Delta}{B - B_{\infty}}\right), \tag{1}$$

where $a_{\mathrm{bg}} = -24.5\ a_0$, $B_{\infty} = 736.8$ G, $\Delta = 192.3$ G [30] and a_0 the Bohr radius. An oscillation of the bias field, $B(t) = \bar{B} + \Delta B sin(\omega t)$, where $\bar{B}$ is the mean and ΔB is the modulation amplitude. This produces an asymmetric $a(t)$ since a is a non-linear function. Thus, the mean is $\bar{a}$, the maximum is a_+, and minimum is a_-.

NUMERICAL METHOD: MCTDHB

The Hamiltonian describing the problem is:

$$\mathcal{H}(t) = \mathcal{T} + \mathcal{V} + \mathcal{W}(t), \tag{2}$$

with $\mathcal{T} = -\frac{\hbar^2}{2m}\sum_i^N \nabla^2_{\mathbf{r_i}}$, $\mathcal{V} = \sum_i^N V_{\mathrm{trap}}(\mathbf{r_i})$ and $\mathcal{W} = \sum_{i<j} W(\mathbf{r}_i - \mathbf{r}_j; t)$ being the many-body kinetic, potential, and interaction energy operators, respectively. We have:

$$V_{\mathrm{trap}}(\mathbf{r}) = \frac{\omega_z^2}{2}z^2 + \frac{\omega_r^2}{2}r^2 \quad \text{and} \tag{3}$$

$$W(\mathbf{r}_i - \mathbf{r}_j; t) = g(t)\delta(|\mathbf{r}_i - \mathbf{r}_j|) = g_0\left[-\beta_1 + \frac{\beta_1}{\beta_2 - \beta_3\sin(\omega t)}\right]\delta(|\mathbf{r}_i - \mathbf{r}_j|), \tag{4}$$

where $g(t)$ and g_0 are dimensionless parameters quantifying the time-dependent and time-independent interaction strengths, respectively, whose values are given below, $\beta_1 = -\beta_2/(\beta_2 - 1) = |a_{bg}/\bar{a}| = 24.5/7.9$, $\beta_2 = |(\bar{B} - B_\infty)/\Delta|$, $\beta_3 = |\Delta B/\Delta|$, and $\mathbf{r} = (x, y, z)^T$. The time-dependent interparticle interaction models the experimental modulation of the scattering length. In the granulation experiment $\omega_r/\omega_z \approx 32$ and so the trap has a cigar shape, close to the 1D regime [35].

To solve the time-dependent Schrödinger equation for many interacting particles,

$$i\hbar\frac{\partial\Psi}{\partial t} = \mathcal{H}(t)\Psi, \tag{5}$$

we apply the Multiconfigurational Time-Dependent Hartree theory for Bosons (MCTDHB) [28, 29] and use the MCTDH-X numerical solver [41–43] for 1D and 3D simulations. The MCTDHB theory assumes a general ansatz $\Psi = \Psi(\mathbf{R}, t)$ for the $N-$particle problem and expands it on a many-body basis $\Psi(\mathbf{R}, t) = \sum_k C_k(t)\Phi_k(\mathbf{R}, t)$, where Φ_k are all possible permanents (i.e. boson-symmetrized many-particle wavefunctions) built over a finite set of M orbitals (i.e. single-particle orthonormal states) $\phi_j(\mathbf{r})$ and $\mathbf{R} = \{\mathbf{r_1}, \mathbf{r_2}, \ldots, \mathbf{r_N}\}$. The theory goes beyond the standard mean-field approximation and incorporates fragmentation and correlation functions of any order p, $1 \leq p \leq N$ [39]. Note that the M orbitals are found self-consistently and are *not a priori* chosen. Therefore, MCTDHB chooses the best set of orbitals at each time. We performed three sets of simulations with the following parameters:

1. A one-dimensional system, with (dimensionless) trap frequency $\omega_{\rm com} = 0.1$, $N = 10^4$, $M = 1$ and $M = 2$ and $g^{(1D)} = g_0(N-1) = 357$. The interaction parameter is found from $g^{(1D)} = 2aN_{\rm exp}\sqrt{\omega_{\rm com}}l_z/l_r^2$, where a is the experimental background value of the scattering length and $l_{r,z} = \sqrt{\hbar/(m\omega_{r,z})}$. The experimental trap frequencies $\omega_r = (2\pi)254$ Hz, $\omega_z = (2\pi)8$ Hz have been used and $\bar{a} = 7.9a_0$, $N_{\rm exp} = 5.7 \times 10^5$ particles (see Eq. 4). The simulations and quantities derived from this dataset are presented in Figs. 7–10. The computation was performed on a 1D spatial grid of 4096 points. The modulating frequencies take on the values $\omega/(2\pi) = 10, 20, 30, \ldots, 90$

Hz. Due to the fast temporal modulation of the atom-atom interaction operator and the resulting strong local density modulations, the computations are numerically highly demanding. Therefore, extended convergence checks are required. We have confirmed convergence with respect to both the spatial grid density and the integration time step as well as error tolerance for frequencies up to $\omega/\omega_z = 10$. Even though the error tolerance demanded is $10^{-11} - 10^{-10}$ (extremely high accuracy) the accumulated error in the total energy at the end of the propagation remains between $3 - 8\%$ and is somewhat larger for the natural occupations. This reflects the fact that the Fock space (spanned by $M = 2$ basis functions) is far from complete [44].

At $\omega/2\pi = 30$ Hz we have seen resonant behavior: the energy increases up to ≈ 10 times after 500 ms and the density is found to occupy all available space. Convergence checks are beyond the computational capacities and the point at $\omega/2\pi = 30$ Hz has not been included in the plots. We attribute the resonant behavior at $\omega/2\pi = 30$ Hz to its proximity to $2\omega_Q$, where $\omega_Q = \sqrt{3}\omega_z$ is the 1D quadrupolar frequency. We have also performed calculations for $\omega_Q = 13.9$ Hz and $2\omega_Q = 27.9$ Hz, and have observed similar behavior.

2. A three-dimensional system with $\omega_z = 1, \omega_y = \omega_x = 32$, $N = 1000$, $M = 1$ and $g^{(3D)} = 4\pi N_{\rm exp} a/l_z = 222$, using also a delta-type interaction pseudopotential. The computational grid was $512 \times 64 \times 64$ wide. All other parameters are set as in paragraph 1. The modulation frequency was set to $\omega = 8.75\omega_z$, that corresponds to the experimental value $\omega/2\pi = 70$Hz. The amplitude of modulation of the interaction is, as before, always positive (results plotted in Fig. 6).

All our simulations use a discrete variable representation. The orbital part of the MCTDHB equations of motion are solved using Runge-Kutta or Adams-Bashforth-Moulton of fixed order (between 5 and 8) and variable stepsize as well as the Bulirsch-Stoer scheme of variable order and stepsize. Davidson diagonalization and short iterative Lanczos schemes were used to evaluate the coefficient part of the MCTDHB equations. The stationary initial state Ψ_0 is found by imaginary time propagation with time-independent interactions,

$g(t) = g_0$. Subsequently, Ψ_0 is propagated in real time for the above time-dependent Hamiltonian and sets of parameter values. For the parameters chosen in the 3D simulation the time unit is $\tau = 19.9$ms and the length unit is $L = 13.5\mu$m. For the 1D simulations we have $\tau = 2$ms and $L = 4.3\mu$m. Energy is measured in units of $\hbar^2/(mL^2)$.

CORRELATION FUNCTIONS, SINGLE SHOT SIMULATIONS, AND CONTRAST

The density matrix $\rho^{(N)} = |\Psi\rangle\langle\Psi|$ describes the N-body quantum system in state Ψ and the reduced density matrix (RDM) of order $p = 1, 2 \ldots$ (partial trace of $\rho^{(N)}$) is most commonly employed and gives the p-particle probability densities. The eigenbasis of the RDMs gives information on the p^{th}-order coherence of the system. In particular, if there is more than one macroscopic eigenvalues of the first (second) order RDM then the system is fragmented and first (second) order coherence is lost.

Specifically, the p^{th}-order reduced density matrix (RDM) is defined as [45]:

$$\begin{aligned} &\rho^{(p)}(z_1, \ldots, z_p | z'_1, \ldots, z'_p; t) \\ &= \tfrac{N!}{(N-p)!} \int \Psi(z_1, \ldots, z_p, z_{p+1}, \ldots, z_N; t) \qquad (6) \\ &\times \Psi^*(z'_1, \ldots, z'_p, z_{p+1}, \ldots, z_N; t) dz_{p+1} \ldots dz_N \\ &= \textstyle\sum_k n_k^{(p)}(t) \phi_k^{(p)}(z_1, \ldots, z_p; t) \phi_k^{(p)*}(z'_1, \ldots, z'_p; t), \qquad (7) \end{aligned}$$

where $n_k^{(p)}(t)$ are its eigenvalues and $\phi_k^{(p)}(t)$ its eigenfunctions. For $p = 1$, $n_k^{(1)}(t) \equiv n_k(t)$ are the so-called *natural occupations* of the corresponding *natural orbitals* $\phi_k^{(1)}(z;t)$. According to the Onsager-Penrose definition [46], a system of N interacting bosons is said to be condensed if and only if one natural orbital $\phi_m^{(1)}$ is macroscopically occupied, or, $n_m/N \sim 1$ for some m, while $n_j/N \sim 0$ for $j \neq m$. If more than one natural orbital is macroscopically occupied then the system is called *fragmented* [47]. The diagonal

$$\rho(z;t) \equiv \rho^{(1)}(z|z;t) = \sum_{k=1}^{M} n_k(t) |\phi_k^{(1)}(z;t)|^2 \qquad (8)$$

we simply call *density*. The eigenfunctions $\phi_k^{(2)}(z_1, z_2)$ of the 2^{nd} order RDM are known as *natural geminals* (NG). Their occupations satisfy $\sum_{j=1} n_j^{(2)} = N(N-1)$ and are plotted in Fig. 9(c) (normalized to 1).

The pth order correlation function is:

$$g^{(p)}(z_1, \ldots, z_p | z_1', \ldots, z_p'; t) = \frac{\rho^{(p)}(z_1, \ldots, z_p | z_1', \ldots, z_p'; t)}{\sqrt{\prod_{i=1}^{p} \rho^{(1)}(z_i, z_i; t) \rho^{(1)}(z_i', z_i'; t)}}. \tag{9}$$

The skew diagonal (antidiagonal)

$$g_{skew}(z, t) = g^{(1)}(z, -z; t). \tag{10}$$

gives the degree of correlation of the density at a point z with its antipodal at point [48] $z' \equiv -z$ (see Fig. 9). Similarly, the normalized pth order correlation function in momentum space can be defined, via the Fourier transform $\tilde{\rho}^{(p)}(k_1, \ldots, k_p | k_1', \ldots, k_p'; t)$ of $\rho^{(p)}(z_1, \ldots, z_p | z_1', \ldots, z_p'; t)$. Note that $|g^{(1)}|$, the spatial correlation function, is bounded like $0 \leq |g^{(1)}| \leq 1$ for any two points (z, z'). For Bose condensed and hence non-fragmented states, $|g^{(1)}|$ takes its maximal value everywhere in space and the state is first-order coherent. Moreover, if $|g^{(2)}| < 1$ we term the state *anticorrelated* while for $|g^{(2)}| > 1$ we term it *correlated*.

The 2^{nd} order correlation function of Fig. 8(a) and Fig. 8(c) for some observed distributions $n(z)$ is given by:

$$C^{(2)}(z, z') = \frac{\langle n(z) n(z') \rangle}{\langle n(z) \rangle \langle n(z') \rangle}. \tag{11}$$

We emphasize that in the expression for $C^{(2)}$, the notation $\langle \cdot \rangle$ corresponds to an average across experimental realizations.

The *single-shot simulations* plotted in Fig. 7(b) and Fig. S1 have been obtained with the method to obtain random deviates of the N-particle probability density $|\Psi|^2$ that is prescribed in Refs. [39, 40]. In brief, the procedure relies on sampling the many-body probability density $|\Psi|^2$ as follows: one calculates the density $\rho_0(z)$, from the obtained solution $|\Psi^{(0)}\rangle \equiv \Psi$ of the MCTDHB equations. A random position z_1' is drawn from $\rho_0(z)$. In continuation, one particle is annihilated at z_1', the reduced density ρ_1 of the

reduced system $|\Psi^{(1)}\rangle$ is calculated and a new random position z_2' is drawn. The procedure continues for $N-1$ steps and the resulting distribution of positions $(z_1', z_2', \ldots, z_N')$ is a simulation of an experimental single-shot image.

The *contrast parameter* $\mathcal{D}$ quantifies the deviation of some spatial distribution $n(z) = n(z;t_0)$ of a single shot at a given time t_0 from the parabolic (Thomas-Fermi-like) best fit $n_{\rm bf}(z) = n_{\rm bf}(z;t_0)$ at the same time and is defined as:

$$\mathcal{D} = \int dz \frac{|n(z) - n_{\rm bf}(z)|}{n_{\rm bf}(z)} \quad \text{or} \tag{12}$$

$$\mathcal{D} = \sum_i^{n_{\rm gp}} \frac{|n(i) - n_{\rm bf}(i)|}{n_{\rm bf}(i)}, \qquad \text{iff} \quad |n(i) - n_{\rm bf}(i)| \geq C_{\rm cutoff}, \tag{13}$$

where i runs over all $n_{\rm gp}$ pixels/grid points. The cutoff requirement $C_{\rm cutoff} = 0.20\ n_{\rm bf}(0)$ is set so that small (zero-excitation) fluctuations are wiped out and only values with large deviations are considered (see Fig. S1). Therefore, the resulting contrast parameter reflects only the large deviations of a given density from its parabolic best fit. To determine the best fits we used the `gnuplot` software to fit the polynomial $p(z) = -a(z-b)^2 + c$, where $a, b, c \in \mathbb{R}$, to the obtained experimental or numerical distributions $n(z)$ along z. The two-dimensional experimental column densities have been integrated along y. The experimental data were also interpolated to a number of points along z so as to equal the grid used for the numerical simulations. An example of a processed image is shown in Fig. S1.

[1] M. C. Cross and P. C. Hohenberg, "Pattern formation outside of equilibrium," Rev. Mod. Phys. **65**, 851 (1993).

[2] M. Faraday, "Xvii. on a peculiar class of acoustical figures; and on certain forms assumed by groups of particles upon vibrating elastic surfaces," Philos. Trans. Roy. Soc. London **121**, 299 (1831).

[3] S. Douady and S. Fauve, "Pattern selection in Faraday instability," EPL **6**, 221 (1988).

[4] R. Keolian, L. A. Turkevich, S. J. Putterman, I. Rudnick, and J. A. Rudnick, "Subharmonic

sequences in the Faraday experiment: Departures from period doubling," Phys. Rev. Lett. **47**, 1133 (1981).

[5] S. Ciliberto and J. P. Gollub, "Pattern competition leads to chaos," Phys. Rev. Lett. **52**, 922– (1984).

[6] S. Ciliberto, S. Douady, and S. Fauve, "Investigating space-time chaos in Faraday instability by means of the fluctuations of the driving acceleration," EPL **15**, 23 (1991).

[7] M. J. Feigenbaum, "The onset spectrum of turbulence," Phys. Lett. A **74**, 375 (1979).

[8] T. B. Benjamin and F. Ursell, "The Stability of the Plane Free Surface of a Liquid in Vertical Periodic Motion," Proc. R. Soc. A **225**, 505 (1954).

[9] J. Bechhoefer and Brad Johnson, "A simple model for Faraday waves," Am. J. Phys **64**, 1482 (1996).

[10] J. J. García-Ripoll, V. M. Pérez-García, and P. Torres, "Extended parametric resonances in nonlinear Schrödinger systems," Phys. Rev. Lett. **83**, 1715 (1999).

[11] K. Staliunas, S. Longhi, and G. J. de Valcárcel, "Faraday patterns in Bose-Einstein condensates," Phys. Rev. Lett. **89**, 210406 (2002).

[12] K. Staliunas, S. Longhi, and G. J. de Valcárcel, "Faraday patterns in low-dimensional Bose-Einstein condensates," Phys. Rev. A **70**, 011601 (2004).

[13] A. I. Nicolin, R. Carretero-González, and P. G. Kevrekidis, "Faraday waves in Bose-Einstein condensates," Phys. Rev. A **76**, 063609 (2007).

[14] R. Nath and L. Santos, "Faraday patterns in two-dimensional dipolar Bose-Einstein condensates," Phys. Rev. A **81**, 033626 (2010).

[15] A. I. Nicolin, "Resonant wave formation in Bose-Einstein condensates," Phys. Rev. E **84**, 056202 (2011).

[16] A. Balaž, R. Paun, A. I. Nicolin, S. Balasubramanian, and R. Ramaswamy, "Faraday waves in collisionally inhomogeneous Bose-Einstein condensates," Phys. Rev. A **89**, 023609 (2014).

[17] H. Abe, T. Ueda, M. Morikawa, Y. Saitoh, R. Nomura, and Y. Okuda, "Faraday instability of superfluid surface," Phys. Rev. E **76**, 046305 (2007).

[18] P. Engels, C. Atherton, and M. A. Hoefer, "Observation of Faraday waves in a Bose-Einstein condensate," Phys. Rev. Lett. **98**, 095301 (2007).

[19] A. Groot, *Excitations in hydrodynamic ultra-cold Bose gases*, Ph.D. thesis, Utrecht University (2015).

[20] L. W. Clark, A. Gaj, L. Feng, and C. Chin, "Collective emission of matter-wave jets from driven Bose-Einstein condensates," Nature **551**, 356 (2017).

[21] B.A. Malomed, *Soliton Management in Periodic Systems* (Springer, 2006).

[22] S. E. Pollack, D. Dries, R. G. Hulet, K. M. F. Magalhães, E. A. L. Henn, E. R. F. Ramos, M. A. Caracanhas, and V. S. Bagnato, "Collective excitation of a Bose-Einstein condensate by modulation of the atomic scattering length," Phys. Rev. A **81**, 053627 (2010).

[23] I. Vidanović, A. Balaž, H. Al-Jibbouri, and A. Pelster, "Nonlinear Bose-Einstein-condensate dynamics induced by a harmonic modulation of the s-wave scattering length," Phys. Rev. A **84**, 013618 (2011).

[24] H. M. Jaeger, S. R. Nagel, and R. P. Behringer, "Granular solids, liquids, and gases," Rev. Mod. Phys. **68**, 1259 (1996).

[25] A. Mehta, ed., *Granular Matter: an Interdisciplinary Approach* (Springer-Verlag New York, 1994).

[26] V. I. Yukalov, A. N. Novikov, and V. S. Bagnato, "Formation of granular structures in trapped Bose-Einstein condensates under oscillatory excitations," Laser Phys. Lett. **11**, 095501 (2014).

[27] V.I. Yukalov, A.N. Novikov, and V.S. Bagnato, "Realization of inverse Kibble–Zurek scenario with trapped Bose gases," Phys. Lett. A **379**, 1366 (2015).

[28] A. I. Streltsov, O. E. Alon, and L. S. Cederbaum, "Role of excited states in the splitting of a trapped interacting Bose-Einstein condensate by a time-dependent barrier," Phys. Rev. Lett. **99**, 030402 (2007).

[29] O. E. Alon, A. I. Streltsov, and L. S. Cederbaum, "Multiconfigurational time-dependent Hartree method for bosons: Many-body dynamics of bosonic systems," Phys. Rev. A **77**, 033613 (2008).

[30] S. E. Pollack, D. Dries, M. Junker, Y. P. Chen, T. A. Corcovilos, and R. G. Hulet, "Extreme tunability of interactions in a ^{7}Li Bose-Einstein condensate," Phys. Rev. Lett. **102**, 090402 (2009).

[31] N. Gross, Z. Shotan, O. Machtey, S. Kokkelmans, and L. Khaykovich, "Study of Efimov physics in two nuclear-spin sublevels of 7li," C. R. Phys. **12**, 4 (2011).

[32] N. Navon, S. Piatecki, K. Günter, B. Rem, T. C. Nguyen, F. Chevy, W. Krauth, and C. Salomon, "Dynamics and thermodynamics of the low-temperature strongly interacting Bose gas," Phys. Rev. Lett. **107**, 135301 (2011).

[33] P. Dyke, S. E. Pollack, and R. G. Hulet, "Finite-range corrections near a feshbach resonance and their role in the efimov effect," Phys. Rev. A **88**, 023625 (2013).

[34] C. C. Bradley, C. A. Sackett, and R. G. Hulet, "Bose-Einstein condensation of lithium: Observation of limited condensate number," Phys. Rev. Lett. **78**, 985 (1997).

[35] C. Menotti and S. Stringari, "Collective oscillations of a one-dimensional trapped Bose-Einstein gas," Phys. Rev. A **66**, 043610 (2002).

[36] S. Stringari, "Collective excitations of a trapped Bose-condensed gas," Phys. Rev. Lett. **77**, 2360 (1996).

[37] M.-O. Mewes, M. R. Andrews, N. J. van Druten, D. M. Kurn, D. S. Durfee, C. G. Townsend, and W. Ketterle, "Collective excitations of a Bose-Einstein condensate in a magnetic trap," Phys. Rev. Lett. **77**, 988 (1996).

[38] *See supplemental material at [URL].*

[39] K. Sakmann and M. Kasevich, "Single-shot simulations of dynamic quantum many-body systems," Nat. Phys. **12**, 451 (2016).

[40] A.U.J. Lode and C. Bruder, "Fragmented superradiance of a Bose-Einstein condensate in an optical cavity," Phys. Rev. Lett. **118**, 013603 (2017).

[41] A. U. J. Lode, "Multiconfigurational time-dependent hartree method for bosons with internal degrees of freedom: Theory and composite fragmentation of multicomponent Bose-Einstein condensates," Phys. Rev. A **93**, 063601 (2016).

[42] E. Fasshauer and A. U. J. Lode, "Multiconfigurational time-dependent Hartree method

for fermions: Implementation, exactness, and few-fermion tunneling to open space," Phys. Rev. A **93**, 033635 (2016).

[43] A. U. J. Lode, M. C. Tsatsos, E. Fasshauer, R. Lin, L. Papariello, P. Molignini, C. Lévêque, and S. E. Weiner, "MCTDH-X: The time-dependent multiconfigurational Hartree for indistinguishable particles software," http://ultracold.org (2019).

[44] Iva Březinová, Axel U. J. Lode, Alexej I. Streltsov, Ofir E. Alon, Lorenz S. Cederbaum, and Joachim Burgdörfer, "Wave chaos as signature for depletion of a bose-einstein condensate," Phys. Rev. A **86**, 013630 (2012).

[45] K. Sakmann, A. I. Streltsov, O. E. Alon, and L. S. Cederbaum, "Reduced density matrices and coherence of trapped interacting bosons," Phys. Rev. A **78**, 023615 (2008).

[46] O. Penrose and L. Onsager, "Bose-Einstein condensation and liquid helium," Phys. Rev. **104**, 576 (1956).

[47] R. W. Spekkens and J. E. Sipe, "Spatial fragmentation of a Bose-Einstein condensate in a double-well potential," Phys. Rev. A **59**, 3868 (1999).

[48] I. Bouchoule, M. Arzamasovs, K. V. Kheruntsyan, and D. M. Gangardt, "Two-body momentum correlations in a weakly interacting one-dimensional Bose gas," Phys. Rev. A **86**, 033626 (2012).

[49] G. Roati, C. D'Errico, L. Fallani, M. Fattori, C. Fort, M. Zaccanti, G. Modugno, M. Modugno, and M. Inguscio, "Anderson localization of a non-interacting Bose–Einstein condensate," Nature **453**, 895 (2008).

[50] E. J. Mueller, T.-L. Ho, M. Ueda, and G. Baym, "Fragmentation of Bose-Einstein condensates," Phys. Rev. A **74**, 033612 (2006).

[51] V. M. Pérez-García, V. V. Konotop, and V. A. Brazhnyi, "Feshbach resonance induced shock waves in Bose-Einstein condensates," Phys. Rev. Lett. **92**, 220403 (2004).

[52] K. J. Thompson, G. G. Bagnato, G. D. Telles, M. A. Caracanhas, F. E. A. dos Santos, and V. S. Bagnato, "Evidence of power law behavior in the momentum distribution of a turbulent trapped Bose-Einstein condensate," Laser Phys. Lett. **11**, 015501 (2014).

[53] N. Navon, A. L. Gaunt, R. P. Smith, and Z. Hadzibabic, "Emergence of a turbulent cascade

in a quantum gas," Nature **539**, 72 (2016).

[54] M. C. Tsatsos, P. E.S. Tavares, A. Cidrim, A. R. Fritsch, M. A. Caracanhas, F. E. A. dos Santos, C. F. Barenghi, and V. S. Bagnato, "Quantum turbulence in trapped atomic Bose-Einstein condensates," Phys. Rep. **622**, 1 (2016).

[55] P. E. S. Tavares, A. R. Fritsch, G. D. Telles, M. S. Hussein, F. Impens, R. Kaiser, and V. S. Bagnato, "Matter wave speckle observed in an out-of-equilibrium quantum fluid," Proc. Natl. Acad. Sci. **114**, 12691 (2017).

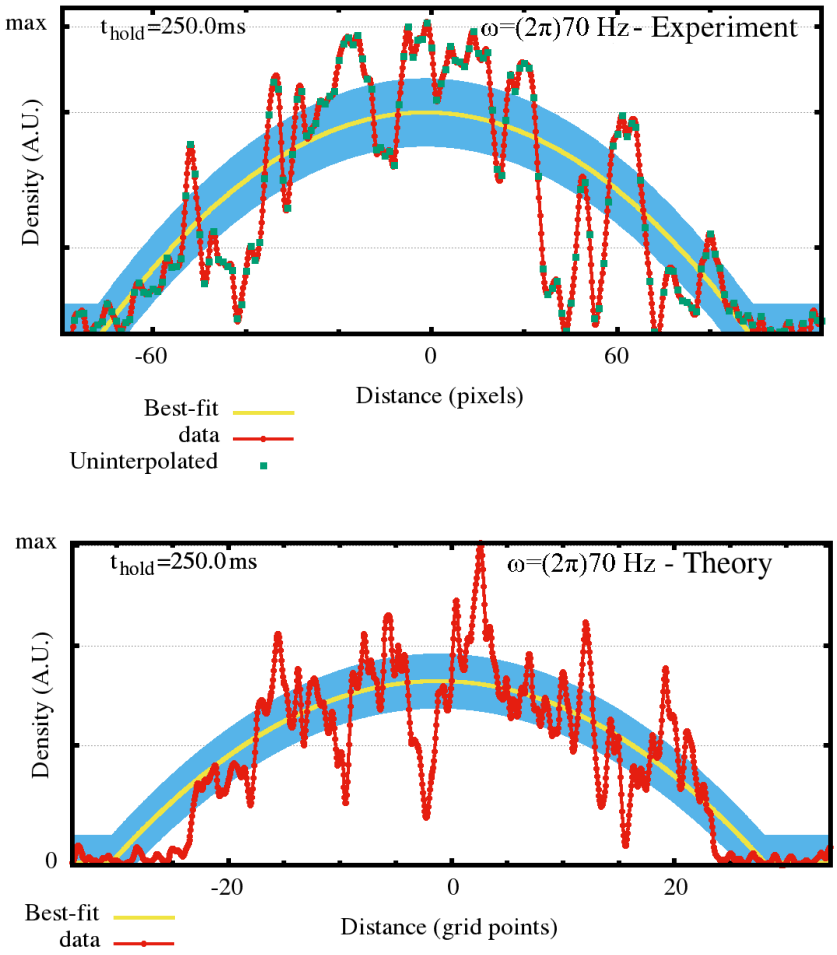

FIG. S1. Example of data fitting. (upper) Experimental and (lower) numerical data are fitted to a parabolic curve (yellow) in order to estimate $\mathcal{D}$ (see Methods). Only values of $\mathcal{D}$ that deviate more than 20% from the value of the fitting function (i.e. points that lie outside the shaded area) are taken into consideration. The images are taken at $\Delta t = t_{\rm mod} + t_{\rm hold} = 250 + 250$ms. The numerical simulation is a 1D model with $N = 10^4$ and $M = 2$ and the grid extension is [-128:128].

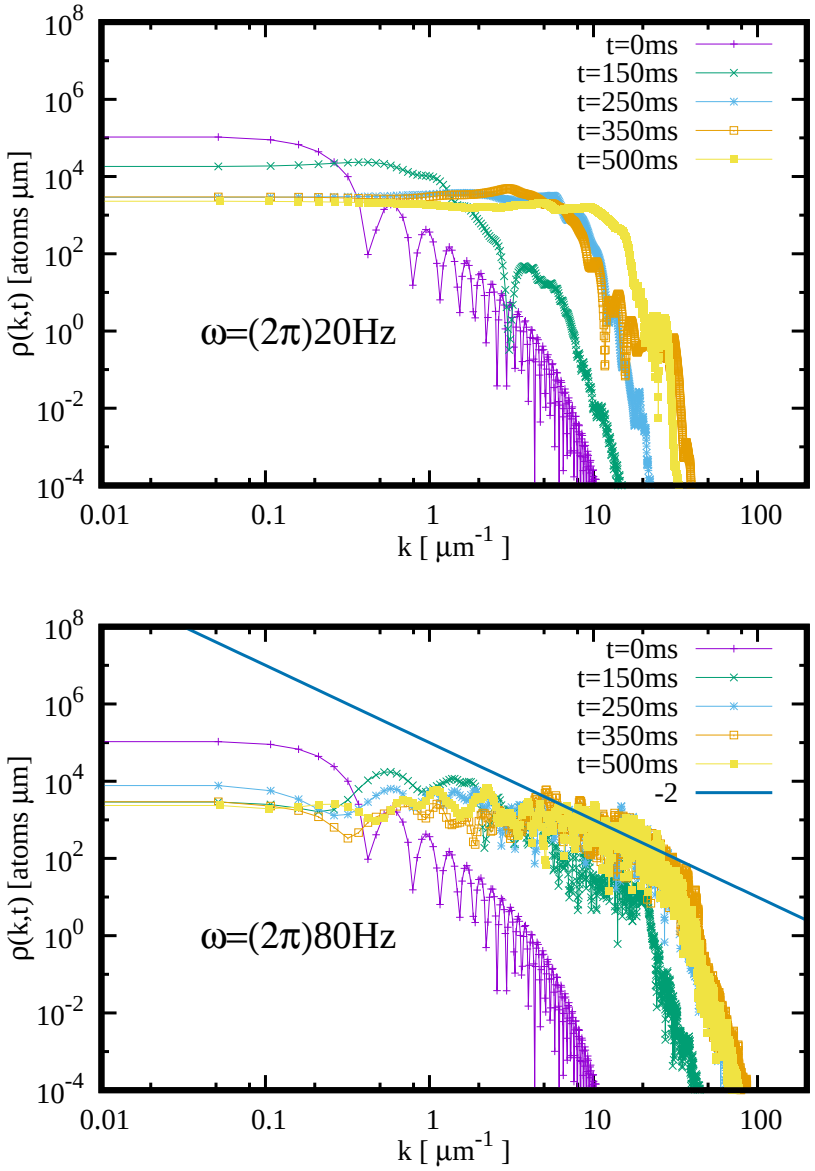

FIG. S2. Density in momentum space. k-space densities for the regular (upper) and the granulated gas (lower panel) as calculated from the MB theory at different times (during modulation for $t \leq 250$ms and after for $t > 250$ms). In the granulated case the momentum distribution scales like k^{-2} (straight line to guide the eye) for almost two decades, behavior that is characteristic of quantum turbulence. Contrary to the regular gas, this scaling remains even 250ms after the modulation.

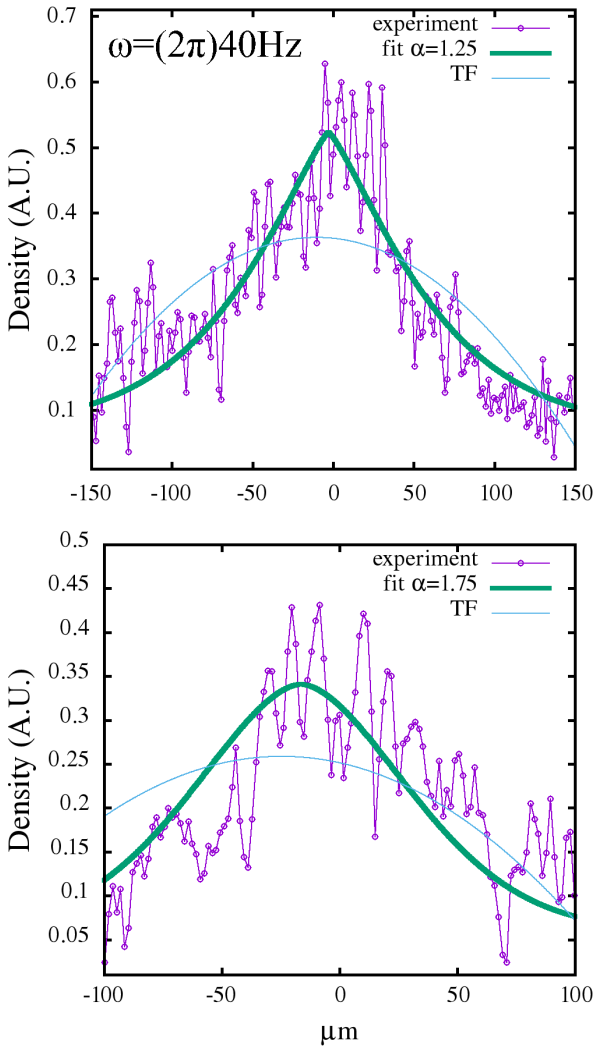

FIG. S3. Experimental column densities exponentially fitted. Close to the threshold frequency $\omega/2\pi = 40$Hz, where the system transitions from regular to granulated states, anomalous spatial distributions are seen (here, two experimental shots for the same initial conditions). These might bear resemblance to localized states, that have been shown to exist in BECs in optical lattices [49]. We fit our observed density distributions to $C + A\exp\left(-\frac{|x-x0|^\alpha}{d}\right)$ and obtain $\alpha = 1.25$ and 1.75 for the two shots. The transition from a regular to a localized states happens as $\alpha \to 1$. For comparison, we plot the parabolic Thomas-Fermi (TF) fit (blue).